Research Article

Induction of Premalignant and Malignant Changes in Nude Mice by Human Tumors-Derived Cell-Free Filtrates

Berlanga-Acosta J[1]*, Mendoza-Mari Y[1], Martinez-Jimenez I[1], Suarez-Alba J[1], Rodriguez-Rodríguez N[1], Garcia-Ojalvo A[1], Fernandez-Mayola M[1], Rosales-Torres P[2], Arteaga-Hernandez E[3], Duvergel-Calderin D[3], Borrajero-Martinez I[3], Campal-Espinosa A[1], Fuentes-Morales D[4], Pimentel-Vazquez E[1], Zamora-Sanchez J[1], Martinez-Suarez JE[3], Estevez-del Toro M[3], Gomez-Cabrera E[5] and Guillén-Nieto G[1]

[1]Center for Genetic Engineering and Biotechnology, Biomedical Research Direction, Ave 31 SN e/158 and 190, Cubanacan, Playa 10600, Havana, Cuba

[2]Department of Pathology, Maria Curie Oncology Hospital, Carretera Central Oeste esquina Madame Curie, Camagüey, CP, 70 700, Cuba

[3]Department of Pathology, Hermanos Ameijeiras Hospital, Calle San Lazaro # 701, Centro Habana, La Habana 10400, Cuba

[4]National Center for Laboratory Animal Breeding, Calle 3ra, No 40759, Entre 6ta y Carretera de Tirabeque, Reparto La Unión, Boyeros, La Habana, Cuba

[5]National Institute of Oncology and Radiobiology, Calle 29 esquina a F, CP 10 400, Vedado, La Habana, Cuba

*Corresponding author: Jorge Berlanga-Acosta, Center for Genetic Engineering and Biotechnology, Ave, 31 S/N, e/158 and 190, Cubanacan, Playa 10600, Havana, Cuba

Abstract

Carcinogenesis is a vast and heterogeneous, multi-step process driven by genetic and epigenetic operators leading to superimposed "tumor organs". Based on our previous experiences of reproducing human donor's histopathological hallmarks in healthy animals exposed to pathologic tissues homogenates, we examined the consequences of administering crude homogenates elaborated from invasive human tumors to nude mice. Subcutaneous administrations of increasing protein concentrations of breast carcinoma homogenates for 6 and 12 weeks, induced lungs atypical adenomatous hyperplasia, foci of lepidic and solid growth poorly-differentiated adenocarcinomas at the two time points. Non-atypical mucosal hyperplasia and adenomas were detected along the gastrointestinal tract. Another experiment addressed the impact of daily administrations (100 µg protein/mouse) of anaplastic sarcoma tissue homogenate for a month. This scheme triggered proliferative changes including: lung adenocarcinomas; a subcutaneous, poorly-differentiated mesenchymal cells tumor, a lymphoadenoma, and multiple gastrointestinal adenomas. When 50% of the month-treated animals were left to evolve treatment-free for other 35 days, a larger and broader incidence of neoplastic changes was found, suggesting autonomous growth: lung adenocarcinomas, a poorly differentiated thyroid tumor, an epithelial tumor within the periaortic brown adipose tissue, and multiple adenomas. These findings indicate that tumor crude homogenates contains soluble "transforming" messengers, that in a short period of time disrupt tissues' proliferative and differentiation programs drifting to progressive neoplasms. This study expands previous evidences on the ability of human pathologic tissues-derived homogenates, to induce the reproduction of diseased donor's histopathologic hallmarks.

Keywords: Cancer; Breast tumors; Sarcoma; Malignant transformation; *In vivo* carcinogenesis; Nude mice; Cells-free filtrate

Abbreviations

CFF: Cells-Free Filtrate (s); IDC: Invasive Ductal Carcinoma (s); CRP: C-Reactive Protein; IL-6: Interleukin-6; TNF-α: Tumor Necrosis Factor-α; VEGF: Vascular Endothelial Growth Factor; MDA: Malondialdehyde; ΔΔCt: Ct Method; RPLE13A: Ribosomal Protein L13a; YWAHZ: Tyrosine 3-Monooxygenase/Tryptophan 5-Monooxygenase Activation Protein Zeta; CEA: Carcinoembryonic Antigen; TTF-1: Thyroid Transcription Factor-1; PPAR-γ: Peroxisome Proliferator-Activated Receptor Gamma; EGFR: Epidermal Growth Factor Receptor; c-Myc: Multifunctional Transcription Factor; PCNA: Proliferating Cell Nuclear Antigen; TGF-α: Transforming Growth Factor Alpha; VEGFR 2: Vascular Endothelial Growth Factor Receptor 2; WBC: White Blood Cell; RBC; Red Blood Cell; LDH: Lactate Dehydrogenase; ALAT: Alanine Aminotransferase; ASAT: Aspartate Aminotransferase; TP53: Tumor Suppressor Protein p53; RB1: Retinoblastoma Protein; EGFR: Epidermal Growth Factor Receptor; CCND1: Cyclin D1 Coding Gene; HIF1A: Hypoxia Inducible Factor 1 Subunit Alpha; BRCA1: Breast Cancer 1; ERBB2: Ligand Orphan Receptor; Member of the Epidermal Growth Factor Receptor Family; AAH: Atypical Adenomatous Hyperplasia; BAT: Brown Adipose Tissue

Introduction

Cancer research dates back to 2,700 years ago [1], and it is likely that the biological foundations of no other human pathology has been so extensively and comprehensively investigated. Cancer is in fact a heterogeneous group of diseases that has remained for years as a major cause of worldwide mortality [2].

The process of cellular malignant transformation entails a sequence of stochastic and non-stochastic events [3] that has enticed, baffled, and discouraged researchers for centuries. By no other means could it be, since carcinogenesis is an enormous-in-size process, that stems from variegated genetic alterations including loss and gain of function mutations that can occur in one single cell [4,5], which runs along stepwise changes from initiation to promotion and progression [6,7], and that translate in enormous cellular resilience for survival, proliferative and dissemination capabilities [8,9]. Cancer cells are also endowed with the singular marks of immortality and autonomy even in adverse tissue ecosystems [1,10]. These cells stripes are able to dedifferentiate [11,12] disguising from their original phenotype, so as to implement transitional reprogramming events from epithelium to mesenchyme [13]. For years, cancer has bewildered pathologists given the hallmarks of atypia, pleomorphism and heterogeneity

[14,15] which are amplified by consecutive adaptations to micro environmental pressures [16,17]. Cancer cells are also gifted with the unusual faculty to locally and remotely invade, colonize, adapt and live in distant tissues, even when the embryonic origin of the metastatic niche may not match with that of primary tumor cells. Ultimately, metastasizing cells enslave the new substrate [18-21]. This multi-faceted process of metastatic seeding has an extremely low mathematical probability (10-8), nonetheless the majority of deaths from solid tumors are caused by metastases [22,23]. Malignant cells also educate the host immune system with lessons of tolerance and ironically use inflammation for their own benefit [11,24]. Finally, cancer cells are actual messages-editing plants, being able to produce and deliver a broad variety of encapsulated or free signals with multiple pathological implications [25,26]. These cancer hallmarks [27,28], has made cancer to immovably remain for years as the emperor of maladies [29].

After Bernard Peyrilhe inaugurated the investigative use of human cancer-derived fluids, the administration to animals of filtered cell-free tumor extracts translated in the groundbreaking discovery of leukemia and sarcoma-causing viruses [30]. We recently undertook the use of cells-free filtrates [31] to examine the hypothesis that the chemical codes of diabetes-related archetypical histopathologic hallmarks in nerves and vessels could be passively transferred to healthy animals, and accordingly reproduce these changes in a way mirroring those of the donor tissues. We therefore envisioned that cells-free filtrate (CFF) could be the vehicle to deliver metabolic memory-associated signalers, acting as driving forces to impose microangiopathy and neuropathy in a normal recipient animal. Having successfully reproduced diabetic vascular pathology in rats [31], CFF were elaborated from lower limb atherosclerotic arteries derived from amputated patients affected with chronic limb ischemia. It was reiteratively observed that CFF inoculation to healthy rats, recreated arteriolar walls histopathological changes typically described for this condition, and identified in the donor subjects (submitted-Frontiers in Cardiovascular Medicine). Once again, the filtered-whole tissue homogenate in a physiological saline solution facilitated the transference of some kind of tissue-derived signal that accounted for the reconstruction of the donor pathology in the host animal.

In line with these notions, and considering that carcinogenesis doctrines entail the combined participation of genomic mutations [32] and epigenetic derangements, as determinants for malignant initiation, progression, and ultimately immortality and autonomy [10,33-35], we embarked on experiments in which healthy nude mice were inoculated with fresh human tumor-cells free filtrates, assuming the hypothetical transference of donor's-derived carcinogenic drivers. We report here that the administration of these tumors crude material is ensued by the onset of progressing premalignant and malignant changes in a narrow temporary window in otherwise normal recipient animals.

Materials and Methods

Ethics and consent

The experimental protocols and the use of human tissues were reviewed and approved by the ethic committees of the National Center for Laboratory Animal Breeding, and Hermanos Ameijeiras Hospital (Havana city, Cuba) respectively. Subjects provided written informed consent for the use of their surgically excised material. These included healthy tissue (dermis and epidermis) serving for control groups, derived from a 42-years old healthy female donor undergoing abdominal cosmetic surgery. Malignant samples used in the study consisted of (1) three mammary invasive ductal carcinomas (IDC) which resulted in high histological grade and intense mitotic index, with lymphatic/vascular permeation, and confirmed invasion of three to five sentinel lymph nodes. (2) A voluminous intrathoracic pleomorphic anaplastic sarcoma that invaded the right hemithorax of a 37-years old female patient. During surgery collected samples were washed with sterile ice-cold normal saline to remove fibrin and debris, and cryopreserved in liquid nitrogen until processing for the CFFs preparation. Tumor samples fragments were as routinely 10% buffered formalin fixed and paraffin processed for histological analysis. The oncologic samples were ultimately processed having received pathologists' report of malignancy.

CFF preparation

Collected tissue was allowed to thaw, weighed and approximately 100 mg of wet tissue were placed in 2 mL vial containing 1 mL of normal saline, homogenized using a Tissue Lyser II for 3 minutes at 30 revolutions per second. Samples were then centrifuged at 10 000 rpm for 10 minutes at 4°C, sterilized by filtration through 0.2 μm nitrocellulose filters (Sartorius Lab Instruments), aliquoted into sterile Eppendorf vials and stored at -70°C. Given the histological similitude of the IDC samples, the three tumors were pooled to ensure larger material availability. Protein concentration was used as the arbitrary unit of measurement to prepare and administer the inoculums.

Characterization of the CFF

Protein concentration (Bicinchoninic Acid Protein Assay Kit. Sigma-Aldrich, USA), and standard commercial ELISA kits for human C-Reactive Protein (CRP), Interleukin-6 (IL-6), tumor necrosis factor-α (TNF- α), and Vascular endothelial growth factor (VEGF) (All from Abcam, Massachusetts, USA) were used according to manufacturer instructions in order to characterize the different tissue-derived CFF. Malondialdehyde was selected as indicator of lipid peroxidation (Lipid Peroxidation Assay Kit, Abcam).

Nucleic acids determination, gene amplification and expression from the tissues homogenates

Two microliters of each CFF were used to determine the DNA and RNA concentrations using a NanoDrop spectrophotometer. The measurement at 260 nm was correlated with nucleic acids concentrations. Total RNA was isolated from 500 μL of each CFF the RNeasy Lipid Tissue Mini kit (Qiagen, Germany). Briefly, 1 mL of Qiazol reagent was added to each sample, mixed by vortex, treated with 200 μL of chloroform and vigorously shaken during 15 seconds. The mixtures were then centrifuged at 12 000 rpm for 15 minutes, 4°C. Upper aqueous phase was transferred to a clean tube and the same volume of 70% ethanol was added and gently mixed. The samples were completely transferred to RNeasy Mini spin columns and washed with 350 μL of buffer RW1. On-column DNase digestion was performed according to Qiagen standard protocol. Subsequently, RNAs were washed with 350 μL of buffer RW1 and twice with 500 μL of buffer RPE. RNAs were eluted in 30 μL of RNase-free water.

Concentration (ng/µL) and quality (260/280 nm ratio) of each RNA were estimated by Nanodrop spectrophotometer. Complementary DNAs were obtained from 50 ng of total RNAs, using Invitrogen SuperScript™ III First-Strand Synthesis SuperMix for qRT-PCR (Invitrogen, Carlsbad, USA) kit, following manufacturer instructions. All cDNAs were diluted 1:10. This methodology was similarly and concurrently applied to corresponding solid tissue samples (pathologic and healthy).

Quantitative PCR reactions were set up in 20 µL using LightCycler® 480 SYBR Green I Master 2x (Roche, Germany) and 300 nM mix of oligonucleotides for each gen (Table 1-Supplemental material). The runs were carried out in a LightCycler®480II (Roche, Germany) and three technical replicas per sample were performed. A standard SYBR Green Probe II program with 45 cycles was used. Reference genes for normalization were chosen according to the stability index after geNorm analysis [36]. Efficiency value for each oligonucleotide pair was calculated by LinRegPCR software (version 11.3) [37]. Fold change for each gen and sample was calculated by REST 2009 [38], using Ct and efficiency values. This software uses the comparative Ct method ($\Delta\Delta$Ct) to analyze data. Gene expression levels were normalized with endogenous control genes YWHAZ (tyrosine 3-monooxygenase/tryptophan 5-monooxygenase activation protein zeta) and RPLE13A (ribosomal protein L13a). For expression levels >1, fold change was considered the same; for expression levels between 0-1, fold change was expressed as -1/expression value. Expression data statistical analysis was performed by REST 2009 software, which uses pair-wise fixed reallocation randomization test. Statistical significance was established for p-values lower than 0.05.

Animals

Female and male BALB/c-Foxn1nu/Cenp mice with 12 to 14 weeks of age were obtained from the National Center for Laboratory Animal Breeding (CENPALAB, Havana, Cuba) and maintained in ventilated racks (Tecniplast, Varese, Italy) in certified rooms for nude mice. Autoclaved food EAO 1004 (CENPALAB, Havana, Cuba) and water were offered ad libitum. Room temperature (20-23°C), humidity (65±10%) and the photoperiod cycles (12 h per day), were automatically controlled. The animals were monitored twice a day by an experienced staff for health problems symptoms. Body weight was registered a day before the study commencement, on a weekly basis and before autopsy. All procedures were performed according to local and International Guiding Principles for Biomedical Research Involving Animals [39]. All animal studies were conducted under a protocol approved by the Institutional Animal Care and Use Committee from the National Center for Laboratory Animal Breeding (CENPALAB), with permit number 07/21.

Experimental protocol I. Lesions induced by breast tumors homogenate: Time-point experiment

This protocol examined the effects of CFF administration derived from high grade IDC breast tumors following 6 and 12 consecutive weeks of administrations. A total of 30 female BALB/c-Foxn1nu/Cenp mice (19-22 g) were randomly distributed among three experimental arms (N=10/arm) receiving: (1) CFF derived from pathological tissue, (2) CFF derived from healthy skin, and (3) physiological saline. Treatments were subcutaneously administered into the interscapular space, once a day, from Monday through Saturday for 6 or 12 weeks.

During the first 6 weeks, the animals received increasing doses of the tissues homogenates: 30, 50, 80, 150, 180 and 200 µg of protein in weeks 1-6, respectively.

At the end of week 6, five mice of each treatment arm were autopsied following standard protocols of our laboratory of pathology. At this point, each animal had received 4.2 mg of protein. The treatments continued thereafter in the other five mice at a fixed dose of 220 µg of protein/mouse, which at the late autopsy point on week 12th had received a total of 12.12 mg of protein. The inoculums and saline were given in volume of 300 µL. Concurrent control groups of mice (healthy skin CFF, and normal saline) received the same inoculation scheme, dosification regimen, and autopsy procedures.

Experimental protocol II: Lesions associated to sarcoma tissue homogenate administration

This protocol aimed to examine the impact of the administration of a highly aggressive sarcoma in mice health. For this purpose 24 BALB/c-Foxn1nu/Cenp male mice (20-23 g) were assigned to either sarcoma or healthy cutaneous tissue homogenates (N=12 for each treatment arm) administrations for 32 consecutive days. Every mouse received 100 µg of protein of each tissue preparation in 300 µL of sterile saline within the interscapular space for an accumulated amount of 3.2 mg/mouse. As we needed to investigate the acute effects of this aggressive scheme and secondly, the eventual evolution of the mice if they were left untreated, 50% of each group (N=6) was destined to an early autopsy study (on day 33), whereas the remaining group was left to evolve untreated for other 35 days for a late autopsy (day 68). Finally, the doses and administration schemes used in these two formal protocols originated from a series of pilot preliminary experiments.

Autopsy, tissue processing and immunohistochemistry

Animals were euthanized under terminal anesthesia. Complete autopsy study was conducted at each experimental time point following an internal protocol based on described techniques [40]. Gross noticeable changes in organs and tissues were recorded, and fragments collected for histopathological analysis. Representative fragments from apparently normal organs were also harvested. Samples were 10% buffered formalin fixed, paraffin-embedded, and serial 5-µm sections stained using H&E. Images were captured using a BX53 Olympus microscope, coupled to a digital camera and central command unit (Olympus Dp-21). Histological examinations were blindly performed by an ad hoc pathologists' board (PRT, EAH, DDC, IBM). Histopathological findings, particularly lungs premalignant and malignant lesions were collectively discussed, and ultimately diagnosed in accordance to current recommendations [41].

Paraffin sections of representative tissue lesions in mice receiving the tumors material, and corresponding specimens from control counterparts, were mounted on poly-l-lysine coated slides (DAKO, California, USA) in order to reduce inter-tissue/experimental variations along immunohistochemistry studies. The slides were dewaxed and rehydrated through graded washes of ethanol. Rehydrated slides were exposed to high pH antigen retrieval solution (DAKO, USA) for 20 minutes at 90°C. Following equilibration at room temperature, slides were washed in PBS and endogenous peroxidase blocked. Unspecific binding blocking solution was used for 20 min and the sections incubated for other 40 minutes with antibodies

directed to: CEA (Abcam, ab133633. 1/1000), TTF-1 (Santa Cruz Biotechnology Sc53136. 1/100), PPAR-γ (Abcam, ab59256. 1/250), vimentin (Abcam, ab92547. 1/250), EGFR (Abcam, ab32077. 1/500), c-Myc (Abcam, ab32072. 1/100), PCNA (Cell Signaling Technology (PC10) Mouse mAb #2586. 1/250), TGF-α (Abcam, ab227723. 1/200), VEGF Receptor 2 (Abcam, ab2349. 1/250). The immunolabeling reaction was developed as described for the Mouse and Rabbit Specific HRP/DAB (ABC) Detection IHC kit (Abcam, ab64264). Non-specific tissue labelling internal controls included the omission/replacement of the primary antibody by the background reducing antibody diluent, and normal rabbit serum (Boster Biological Technology, Pleasanton CA, USA, catalog # AR1010).

Blood analysis

Under deep anesthesia at the moment of autopsy, approximately 400 μl of blood were collected from the femoral vein and placed in small sample tubes containing ethylenediaminetetraacetic acid (40 μL/mL of total blood) for hematological analysis. Parameters analyzed included hemoglobin concentration, hematocrit, WBC count and differential, platelets, and RBC counts. Neutrophil/lymphocyte ratio was calculated. Measurements were done in an automated hematology analyzer MICROS ABX (Roche Diagnostic Systems). Similar amount of non-anticoagulated blood was used for hemochemistry parameters as total proteins, glycemia, LDH, ALAT and ASAT, which were determined from serum using a Cobas Integra 400 PLUS automatic analyzer (Roche DiagnosticSystems). Data were processed using GraphPadPrism 6 (GraphPad Software, San Diego, CA). Kolmogorov-Smirnov and Levene's tests were used to assess data normality and variance homogeneity. If data were in compliance with normal distribution and variance homogeneity, comparisons between groups were carried out using the Student's unpaired t test. Otherwise, Mann Whitney test was performed. Statistically significant differences were established for p≤0.05.

Results

Cells-free filtrate biochemical characterization

As mentioned above, these experiments used three varieties of fresh human tissues as surgical specimens to prepare the crude CFF: healthy skin, mammary invasive ductal carcinoma, and a portion of an aggressive intracavitary sarcoma. As shown in Table 2, the three tissue samples rendered sufficient protein concentration for the study protocols administration regimens. An elemental biochemical description of the three tissue type homogenates suggests that: (1) the accumulation and activity of membrane peroxidated polyunsaturated fatty acids is similar between the healthy and the tumor tissue samples, (2) the sarcoma-derived CRP content was 3.8 and 4.8 superior than the concentration calculated for the pool of mammary tumors and the healthy skin, respectively, (3) the tumor samples seem to exhibit a particular inflammatory signature. Mammary tumors pool shows the largest concentration of IL-6, paradoxically, this reactant is fairly low in sarcoma sample. In turn, TNF-α sarcoma-derived homogenate concentration surpasses 15-fold the values calculated for the healthy skin and the mammary tumors homogenates. Finally, both tumor variants largely exceed VEGF concentration as compared to healthy skin. Of note, the concentration measured in the mammary tumors pool surpasses 50 and 200 folds the values registered for the sarcoma and the healthy skin respectively.

Cells-free filtrate genetic characterization

Spectrophotometric measurements at 260 nm indicated that both pathological CFF contained DNA and RNA at similar concentrations. Although RNA extraction, reverse transcription and amplification from the sarcoma-derived CFF, rendered non-reproducible results, RNA was successfully reverse-transcribed to give rise complementary DNA molecules using the pool of mammary carcinomas homogenate. Thus, data shown in Table 3 correspond to the breast tumors pool CFF. Nucleic acids appeared to tolerate the mechanical process in Tissue Lyser machine for solid tissues disruption. Purified RNA concentrations were between 9.2-9.4 μg/μL, with a total yield of 270 ng every 500 μL of CFF used for purification. Even though the concentration of total RNA was low, the A260/A280 ratio was estimated between 1.8 and 2, which was useful for subsequent reactions. As expected, RNA directly recovered from solid tumor and healthy skin tissue showed higher concentrations (40.3 and 57.3 μg/μL, respectively) and also the appropriate quality for qPCR studies. The amplification efficiencies of genes in study were very similar, all ranged between 1.895 and 1.990. Among six endogenous reference genes tested, RPLE13A and YWAHZ showed to be the most stable; therefore they were used for normalization during the expression study by using the REST 2009 software.

Solid breast tumors expressed significantly higher levels for all the marker genes in study as compared to healthy skin tissue (Table 3, p<0.0001). These included MYC, TP53, RB1, EGFR, CCND1, HIF1A, BRCA1 and ERBB2. For the CFF samples, there was a significant elevation of BRCA1 and RB1 expression in tumor-derived homogenate as compared to healthy skin (p<0.0001 and p<0.05, respectively). Although non-statistically significant, fold change values obtained for TP53, CCND1 and HIF1A were higher for tumor sample related to healthy skin. Curiously, this homogenate tumor sample showed a non-statistically significant decrease of MYC expression (-9.43-fold) compared to healthy skin. EGFR and ERBB2 genes couldn't be amplified from CFF-derived RNAs (Table 3).

Experimental protocol I: Lesions induced by breast tumors homogenate

From the clinical point, mice receiving the breast IDC homogenate began to show a tendency to fatigue and lethargy from week 4th onward when had individually received 1.8 mg of pathologic material-derived protein. This behavioral change remained unmodified until 12th week autopsy. Mice also showed a leaner appearance and dry skin. Of note, however, these alterations were not associated to significant body weight modifications on 6th week autopsy point, when compared to healthy material recipient mice (19.14 ± 2.42 vs. 18.33 ± 1.4. p=0.98). Mice receiving normal skin CFF exhibited a healthy aspect and a normal behavior with no lethargy or activity depression. Six weeks of treatment with tumors-derived material appeared to alter hematological homeostasis with significant elevation in hemoglobin levels and erythrocytes count. Furthermore, there was a significant increase in the percentage of circulating polymorphonuclear cells paralleled by lymphocytes reduction (Table 4). Blood chemistry parameters as glycemia, total proteins, ASAT, ALAT, and LDH were similar between the tumors homogenate group, and the matched control animals (data not shown).

Completing 6 weeks of treatment representing 4.2 mg of protein/

Table 1: Genes and primers information (supporting information).

Gene symbol	Gene name	Accession no.	Oligo	Sequence	PCR product size (bp)
RPLE13A	Ribosomal protein L13a	NM_012423.4	Forward	GGCCCAGCAGTACCTGTTTA	93
			Reverse	AGATGGCGGAGGTGCAG	
YWAHZ	Tyrosine 3-monooxygenase/tryptophan 5-monooxygenase activation protein zeta	NM_145690.2	Forward	GCTCCTCAAGAGCAGGGACAAT	100
			Reverse	TCAAGACTCACTGCCTCCCATC	
MYC	MYC proto-oncogene, bHLH transcription factor	NM_002467.6	Forward	AGGCTCCTGGCAAAAGGTCAGA	122
			Reverse	CGCTGCGTAGTTGTGCTGATGT	
TP53	Tumor protein p53	NM_000546.6	Forward	GGCTCTGACTGTACCACCATCCA	146
			Reverse	ACACGCACCTCAAAGCTGTTCC	
CCND1	Cyclin D1	NM_053056.3	Forward	GCAGACCTTCGTTGCCCTCTGT	120
			Reverse	TTGTTGGGGCTCCTCAGGTTCA	
HIF1A	Hypoxia inducible factor 1 subunit alpha	NM_001530.4	Forward	CCACCTATGACCTGCTTGGTGC	103
			Reverse	CCAGGCTGTGTCGACTGAGGAA	
BRCA1	BRCA1 DNA repair associated	NM_007294.4	Forward	GGGCCACACGATTTGACGGAAA	137
			Reverse	GCTGACTCTGGGGCTCTGTCTT	
RB1	RB transcriptional corepressor 1	NM_000321.3	Forward	TTGCAGTATGCTTCCACCAGGC	101
			Reverse	CCTCCAGGAATCCGTAAGGGTGA	
EGFR	Receptor for epidermal growth factor	NM_005228.5	Forward	GTGGATGCCGACGAGTACCTCA	147
			Reverse	GGGACAGCTTTGCAGCCCATTT	
ERBB2	Erb-b2 receptor tyrosine kinase 2	NM_004448.4	Forward	TGACCTGCTGGAAAAGGGGGAG	147
			Reverse	CTGGCCATGCGGGAGAATTCAG	

Table 2: Descriptive biochemical characterization of the cells-free filtrate samples.

CFF Samples	Protein yield (mg/mL)	MDA/mg prot. (nmol/mg)	CRP/mg prot. (ng/mg)	IL-6/mg prot. (pg/mg)	TNF-α/mg prot. (pg/mg)	VEGF/mg prot. (pg/mg)
Healthy skin	1.71	0.135	14.04	0.326	3.43	6.34
Breast tumors	2.22	0.316	20	19.41	2.2	1286.98
Anaplastic sarcoma	0.85	0.397	67.66	1.32	51.92	25.45

MDA: Malondialdehyde; CRP: C-Reactive Protein; IL-6: Interleukin 6; TNF-α: Tumor Necrosis Factor; VEGF: Vascular Endothelial Growth Factor.

Table 3: Relative gene expression of tumor marker genes in solid tissues and CFF samples as compared to healthy skin.

Gene	Breast tumor tissue *vs.* healthy skin				Breast tumors CFF *vs.* healthy skin			
	Reaction Efficiency	Expression	P(H1)	Result	Reaction Efficiency	Expression	P(H1)	Result
MYC	0.922	2.969	0	UP	0.922	0.106	0.082	
TP53	0.908	2.469	0	UP	0.895	1.516	0.221	
RB1	0.924	6.829	0	UP	0.925	3.379	0	UP
EGFR	0.942	6.883	0	UP	NA			
CCND1	0.94	2.151	0	UP	0.965	1.383	0.105	
HIF1A	0.94	10.91	0	UP	0.948	3.557	0.085	
BRCA1	0.99	4.924	0	UP	0.985	2.17	0.033	UP
ERBB2	0.901	8.531	0	UP	NA			

Relative gene expression was measured as the fold change of the genes related to endogenous reference genes (RPLE13A and YWAHZ) using REST 2009 software. P(H1): Probability of alternate hypothesis that difference between sample and control groups is due only to chance. NA: Not Amplified.

animal were sufficient to induce proliferative non-malignant, premalignant, and malignant changes especially in the lungs of the IDC recipient mice. Lungs microscopic examination in all these mice revealed multifocal areas of parenchymal condensation, consisting of atypical adenomatous hyperplasia (AAH) at the expenses of type 2 pneumocytes with clear, enlarged, and atypic nuclei, along with multifocal nodules of solid or lepidic growth patterns adenocarcinomas (Figure 1A), positive to CEA immunolabeling (Figure 1B). In contrast, mice treated with the healthy skin CFF showed lungs with normal parenchymal histology and no CEA expression (Figure 1C and 1D). IDC homogenate administration for 6 weeks was also associated to gastric and intestinal mucosal

Table 4: Hematological parameters upon 6 and 12 weeks of mammary tumors homogenate administration (supporting information).

6 weeks of treatment			
Parameters	**Breast tumors**	**Healthy skin control**	**p**
Hemoglobin (g/dL)	11.74 ± 0.79	9.58 ± 1.67	0.031
RBC (10^6/mm³)	10.12 ± 1.37	7.77 ± 1.58	0.0368
WBC (10^6/mm³)	5.44 ± 2.54	3.70 ± 0.70	0.213
Hematocrit (%)	39.10 ± 4.68	30.72 ± 7.13	0.0593
Neutrophils (%)	43.20 ± 11.39	27.60 ± 9.13	0.0438
Lymphocytes (%)	54.80 ± 12.03	70.80 ± 9.50	0.0478
Neutrophil/Lymphocyte Ratio	0.87 ± 0.480	0.41 ± 0.19	0.041
12 weeks of treatment			
Parameters	**Breast tumors**	**Healthy skin control**	**p**
Hemoglobin (g/dL)	11.58 ± 0.46	11.70 ± 1.46	0.866
RBC (10^6/mm³)	10.12 ± 0.60	10.16 ± 1.37	0.947
WBC (10^6/mm³)	9.30 ± 5.63	6.04 ± 1.66	0.4034
Hematocrit (%)	40.52 ± 2.73	42.00 ±6.23	0.64
Neutrophils (%)	56.20 ± 21.42	60.40 ± 11.95	0.712
Lymphocytes (%)	42.20 ± 19.47	39.00 ± 12.10	0.763
Neutrophil/Lymphocyte Ratio	1.54 ± 1.18	1.89 ± 0.52	0.564

RBC: Red Blood Cells. WBC: White Blood Cells. Data are presented as the mean ± standard deviation. Statistical analyses were performed using the Student's unpaired t test. p≤0.05 was considered as significant.

Table 5: Major histopathological changes identified in animals treated with tumor tissues-derived homogenates.

| Experimental protocol I. Lesions induced by breast tumors homogenate. 6th week autopsy	
Proliferative changes	**Incidence**
Atypical adenomatous hyperplasia	5/5
Foci of lepidic growth adenocarcinoma	3/5
Diffuse nodules of invasive, poorly differentiated solid adenocarcinoma	5/5
Antral adenoma	1/5
Colon villous adenoma	1/5
Experimental protocol I. Lesions induced by breast tumors homogenate. 12th week autopsy	
Diffuse nodules of invasive, poorly differentiated solid adenocarcinoma	5/5
Gastrointestinal mucosa hyperplasia	5/5
Gastric adenomas	4/5
Colon papillary adenomas	2/5
Protocol II. Administration of CFF derived from an anaplastic pleomorphic sarcoma. Early autopsy (Day 33)	
Alveolar septal cells hyperplasia (type 2 pneumocytes)	6/6
Lung adenocarcinoma (solid pattern)	1/6
Gastrointestinal mucosa hyperplasia	6/6
Gastric adenomas	2/6
Colonic villous or papillary adenomas	5/6
Foci of ectopic intestinal mucosal duplication	3/6
Inter-scapular nodule made up poorly-differentiated cells of putative mesenchymal origin	1/6
Lymphoadenoma	2/6
Protocol II. Administration of CFF derived from an anaplastic pleomorphic sarcoma. Late autopsy (Day 68)	
Lung diffuse adenocarcinomas of solid growth pattern	3/6
Lung metastasis made up by poorly differentiated epithelial	3/6
Undifferentiated tumor of in thyroid gland	1/6
Brown adipose tissue transformation with epithelial cells and an epithelial tumor with glandular differentiation	2/6
Gastric mucosa hyperplasia	6/6
Small and large bowel mucosal glandular hyperplasia and dysmorphia.	4/6
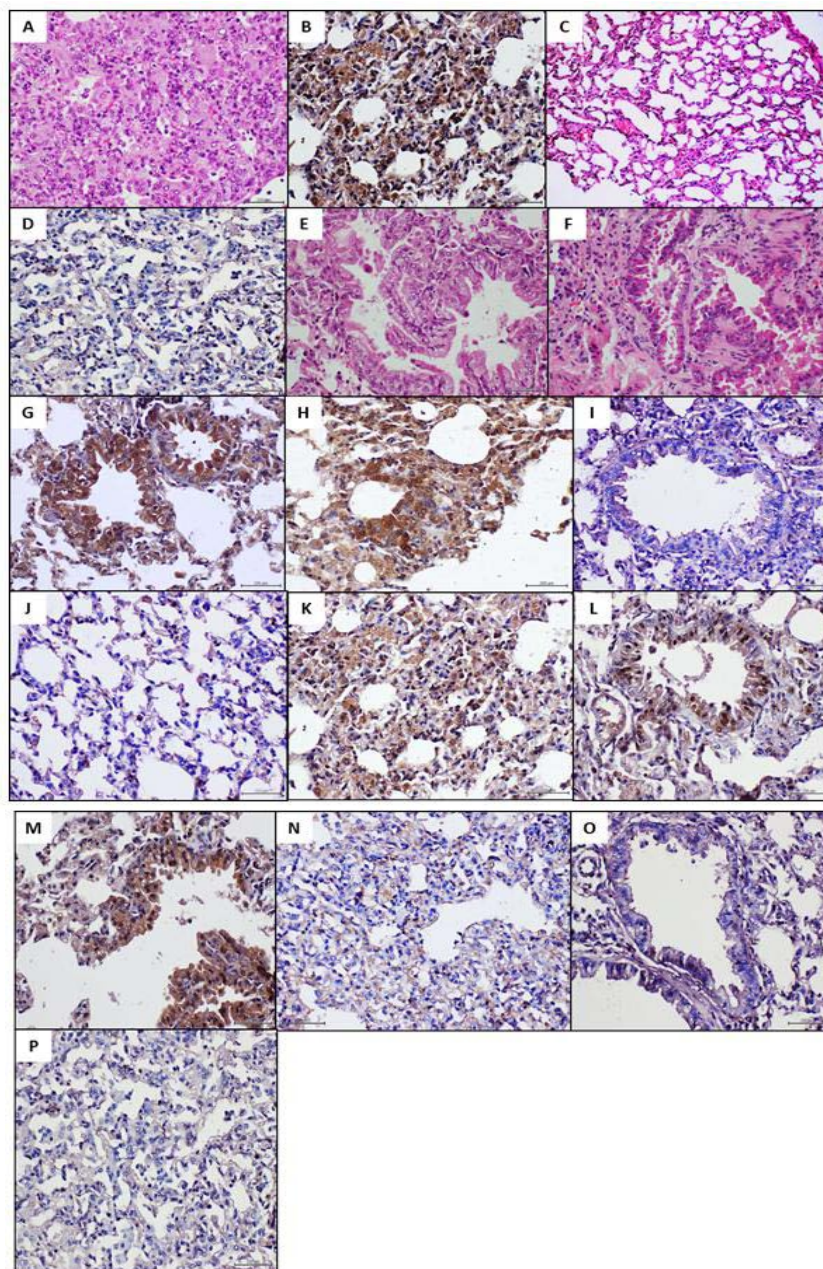
Figure 1: Histological and immunohistochemical characterization of lungs specimens from mice exposed to invasive breast tumors homogenate. A: H/E staining of solid adenocarcinoma following 6 weeks of treatment with IDC. B shows intense immunohistochemical reactivity to CEA expression. Normal lung parenchyma histology from a control animal is shown in C. D: Lungs from control mice showed no CEA expression. E: Lung adenocarcinoma of lepidic growth with abundant atypical alveolar and bronchiolar epithelial cells in a mouse treated for 12 weeks. F: Appearance of a lung normal histology in a concurrent control mouse. G: Atypical bronchiolar cells of a lepidic adenocarcinoma showing intense immunoreactivity to EGF receptor. H: Similarly, VEGF receptor-2 was also conspicuously expressed by atypical bronchiolar and septal cells. Mice treated for 12 weeks with breast tumors material. I and J: EGF and VEGF receptors were expressed by bronchiolar and septal cells to far less intensity in lung specimens from 12-weeks matched control mice. K, L and M are representative of malignant cells intense immunoreaction to C-Myc, PCNA, and TGF-α expression in lungs from mice treated with the breast tumors homogenate for 12 weeks. N, O and P demonstrate that C-Myc, PCNA and TGF-α are physiologically expressed by septal and bronchiolar epithelial cells in normal lungs from 12 weeks matched control mice. The expression of these markers is consistently lower than that found in lungs from tumors-treated mice. All 5μm sections. Magnification x40. Scale bar 200μm.

hyperplasia with no evidence of cellular/nuclear atypia (not shown).

Mice exposed for 12 weeks to breast tumors CFF continued with an abnormal, diseased-like behavior but with no significant changes in body weight as compared to the control counterpart (20.55 ± 2.359 *vs.* 21.02 ± 1.74, p=0.89). At this time point (Table 4), statistical differences were neither detected for hemoglobin levels, erythrocytes and WBC counts, nor for the percentage of circulating polymorphonuclear cells and lymphocytes. In general terms, the initial hematologic derangements at 6th week, appeared reverted on the late autopsy point (Table 4). Similar to week 6, the analysis of blood chemistry parameters showed no significant alterations in
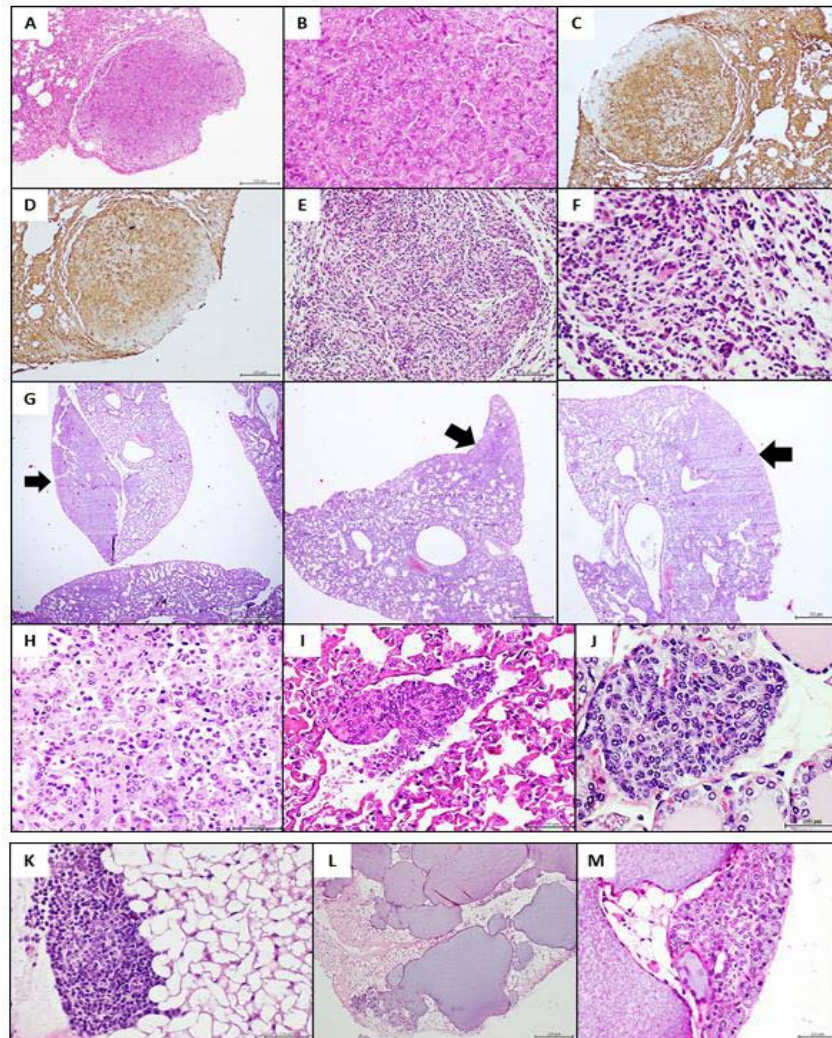
Figure 2: Histological and immunohistochemical characterization of mice malignancies following treatment with an aggressive sarcoma homogenate. Early and late autopsies findings. A: Lung solid tumor nodule detected at the early autopsy time point. B: The tumor is exhibiting poorly-differentiated epithelial cells with vacuolated cytoplasm, vesiculous nuclei and prominent nucleoli. C and D: The lesion was conclusively indicative of a poorly differentiated adenocarcinoma immunoreactive to CEA and TTF-1, respectively. E: Inter-scapular nodule in the BAT at the administration site in a mouse examined on the early autopsy time point. F shows the nodule is made up by proliferative, poorly-differentiated fusiform and round cells of putative mesenchymal origin. Osteoblast-like multinucleated giant cells, cellular and nuclear atypia, cellular disorder and cells with tadpole-like cytoplasm are observable. The lesion was interpreted as a tumor of poorly differentiated mesenchymal cells and was detected at the early autopsy point. Mice treated with the sarcoma homogenate for 32 days and left to evolve free-of-treatment for other 35 days –late autopsy point. G: Low power (x4) images of three mice lungs showing areas of parenchymal consolidation, microscopically concluded as poorly-differentiated adenocarcinomas as representatively illustrated in H.
I: A metastatic nest of tumoral cells corresponding to a mouse examined at the late autopsy point. The colony is made up by poorly differentiated epithelial cells grouped within the luminal aspect of a lymphatic vessel indicative of a metastatic invasion. J: At this point, a thyroid gland tumor made up by undifferentiated round cells with pleomorphic nuclei and prominent nucleoli was detected. Two mice corresponding to late autopsy group showed a disruption in periaortic/mediastinal BAT homeostasis. K: The normal multifocal subcortical aggregates of round, blue, undifferentiated cells of non-lymphoid aspect that progressively originate mature adipocytes; turned to originate island-like inclusions of epithelial cells with formation of tubular structures of acinar aspect, mucosecretory, and PAS positive material in cystic lakes formations as shown in L. M: These epithelial cells exhibit pleomorphic malignant nuclei and reinforced nuclear membrane suggesting an epithelial tumor with glandular differentiation. H/E. Magnifications x4, x10, x40. Scale bar 200µm.

animals receiving the malignant material as compared to control groups (not shown).

As depicted in Table 5, lungs of the five animals receiving the tumors material for 12 weeks exhibited almost massive parenchymal condensation, and alveolar lumen erasing due to invasion of multinodular, solid and lepidic growth adenocarcinomas (Figure 1E). Accordingly, the initial areas of AAH had transformed in authentic

invasive and scattered tumors. Mice treated with the healthy skin homogenate showed a morphologically normal parenchyma (Figure 1F). Pathologic lungs specimens immunohistochemistry reproducibly indicated that both EGF and VEGF receptors were intensely expressed (Figures 1G and 1H); in sharp contrast to the discrete immunolabeling detected in control normal lungs (Figures 1I and 1J). Furthermore, the pathologic specimens also showed strong

signal for c-Myc, PCNA and TGF-α in atypical septal and bronchiolar epithelial cells (Figure 1K, 1L and 1M), whereas far less conspicuous and more circumscribed was the expression for these markers in normal lungs from the healthy skin control group (Figure 1N, 1O and 1P).

Experimental protocol II: Lesions associated to sarcoma tissue homogenate administration

As previously anticipated, the main goal of this protocol was to examine the impact of an aggressive mesenchyme-derived tumor, and to learn about the outcome of putative lesions resulting from a month of treatment in animals left untreated for other 35 days. Thus, we basically focused to discern what the prevailing outcome was: regression or progression. Sarcoma-derived CFF did not affect animals' body weight after a month of treatment as compared to healthy skin-derived homogenate's recipients (19.6 ± 1.27 vs. 19.02 ± 1.05, p=0.24). Body weight was also indifferent at the end of the non-treatment period of 35 days (21.02 ± 0.78 vs. 20.71 ± 1.11, p=0.27). Along this phase, animals appeared slightly clumsy but with a healthy somatic aspect. The flaky and dry skin appearance induced by the mammary tumors homogenate was not observed in sarcoma-treated mice.

Administration of the sarcoma-derived material impacted a variety of organs of both epithelial and mesenchymal nature. As shown in Table 5, its effects translated in non-malignant, pre-malignant and malignant proliferative changes that involved lungs, gastrointestinal mucosa, thyroid gland, and brown adipose tissue (BAT). The 32 days of uninterrupted administration of the sarcoma CFF (totalizing 3.2 mg of protein/mouse), induced massive alveolar septal cells and gastrointestinal mucosal hyperplasias with no evidences of cellular/nuclear atypia. Noteworthy is however, the high incidence of gastric and colonic adenomas (Table 5) that included glandular hyperplasia, dysmorphia, and Goblet cells hyperplasia. Furthermore we also registered the presence of serosal nodules of ectopic duplication of intestinal tissue alone, or associated to lymphoid cells (Table 5). The most remarkable findings in this autopsy point were: a round and well-consolidated lung nodule of malignant, poorly differentiated cells, positive to CEA and TTF-1, concluded as an adenocarcinoma (Figure 2A-2D), and a subcutaneous nodule in the BAT at the interscapular space (injection site), made up by poorly-differentiated fusiform, round, tadpole-like and multi-nucleated cells of putative mesenchymal origin, being concluded as a tumor of poorly differentiated mesenchymal cells (Table 5 and Figure 2E, 2F).

When mice were left untreated for 35 days, lungs and other tissue lesions progressed to authentic tumors. Thus, lesions incidence increased and carcinogenesis seemed to proceed (Table 5). Three animals exhibited diffuse areas of lung parenchymal condensation (Figure 2G), due to diffuse nests of invasive and poorly differentiated lung adenocarcinomas (Figure 2H), while another mouse showed a lump of malignant, poorly differentiated epithelial cells that impressed a metastatic colony allocated within the luminal aspect of a lymphoid vessel (Figure 2I). Furthermore, the invasive adenocarcinomas in a similar manner to those described in mice receiving the mammary tumors CFF, proved to intensely express bona fide-malignant transformation markers as c-Myc, TGF-α, PCNA, EGF and VEGF receptors as compared to limited expression found in control animals

treated with the healthy skin homogenate (not shown). Thyroid gland showed a microscopic undifferentiated tumor of atypical round cells with pleomorphic nuclei and prominent nucleoli (Figure 2J). Sarcoma CFF administration seemed to interfere with BAT cells differentiation program. Multifocal aggregates of subcortical, round, blue, undifferentiated BAT precursors cells negative to vimentin and PPAR-γ expression (not shown), and ordinarily detected in mediastinal and periaortic niches (Figure 2K), showed to progress through a phenotypic and structural reprogramming; giving rise to island-like inclusions of epithelial cells with formation of tubular structures of acinar mucosecretory aspect, and PAS positive mucin lakes. These epithelial cells exhibited pleomorphic malignant nuclei and a reinforced nuclear membrane, suggestive of an epithelial tumor with glandular differentiation (Figure 2L and 2M). Sarcoma CFF also induced gastrointestinal glandular and epithelial hyperplastic response with no histologic evidences of malignancy. Finally, none of the described alterations were detected along the macro and microscopic examination of the healthy skin control animals.

Discussion

We show here that human malignant tissues-derived homogenates contain messengers or signalers that are able to disrupt the growth and differentiation homeostasis of host cells in otherwise healthy animals. Accordingly, the administration of these soluble "malignant signalers" imposes the pathologic condition of the donor through the induction of premalignant and genuine malignant changes. Of note, the pathologic alterations observed in our animals were associated to the tumors-derived CFF which were simple, crude, whole tissue homogenates using sterile physiologic saline solution with no purification processes or any type of chemical manipulation. Thus, these homogenates represent a pure extract of the tissues, a rich-in-content material and a vehicle of donor cells' soluble signatures.

The fact that none of these alterations were ever detected at the organ, tissue, and cellular levels in any of the control animals, suggests that there was no spontaneous tumorigenesis during the experimental period, and that the neoplastic traits observed, do not represent a form of tissue reactive response to the human xenogeneic material. This assertion is also supported by the observation that tumors-homogenates pathologic changes entailed proliferation and differentiation alterations, devoid of an associated immune-inflammatory response.

For these experiments examining the hypothetical existence of a soluble and transferable "tumor tissue memory", two prototypes of emblematic cancers of epithelial and mesenchymal origin were selected: invasive ductal mammary carcinoma, and an aggressive, highly proliferative, pleomorphic sarcoma. Breast cancer is a high incidence-epithelial tumor and the global leading cause of cancer death among females [42]. Although sarcomas are rare human malignancies, this heterogeneous family of tumors is the second most common type of solid tumors [43]. These are mesenchyme-derived, ordinarily proliferative and invasive tumors [44,45].

Breast IDC and sarcoma-derived homogenates transformed cells and consequently acted as legitimate carcinogens. Breast cancer homogenate affected 100% of the animals with lung tumors, being its effect primarily circumscribed to that epithelial organ. This material

transiently affected the hemo-lymphopoietic response, abated animals' activity, and faded somatic and cutaneous appearance, although their-sick aspect was not reflected in body weight reduction. Sarcoma-derived CFF, however, exhibited a broader activity spectrum as organs of epithelial and mesenchymal origin were impacted. We deem that the biological nature of each tumor and the imprinting of its individual signature in recipient animals, may explain the differences observed in the spectrum of induced pathologies. The initial descriptive biochemical characterization of tissue samples suggests differences in cytokines profiles for each tumor variant. Aside from differences, nevertheless, both tumor filtrates targeted the lungs and induced invasive adenocarcinomas positive to broadly-validated lung tumor markers [46,47] in only 4 to 6 weeks. These observations incite to question about what drivers could be underpinning the lung tissue tropism described for both carcinoma and sarcoma-recipient mice, and what forces could be propelling the rapid tumors growth, assuming they transited along the canonic multistep cascade of initiation-promotion-progression.

As described above, the initial diffuse areas of lungs AAH progressed to malignant processes under permanent treatment with breast tumors CFF between weeks 6th to 12th; consequently, transforming the lungs in oversized adenocarcinomas and confirming the precursor character of AAH [48]. The fact that the treatment-free period conceived in the sarcoma-based protocol, acted as the timeframe for lungs and other organs' lesions to evolve and progress with inducer-independency, is biologically meaningful given that the treatment was limited to 4 weeks. This evidence motivates to hypothesize that these lesions were authentic neoplasms from their early time point, and that had established and accumulated sufficient "self-capabilities" for an irreversible and autonomous progression. We can assume therefore, that these lesions meet critical traits considered as cancer hallmarks by Hanahan and Weinberg [28]. This assumption is further supported by the existence of a metastatic colony of malignant epithelial cells in this group. Metastasis is a cancer hallmark [28] being considered the last step in the multistep process of tumor progression [28,49].

The immunohistochemical results lend additional substantiation to the hypothesis of self-sufficiency for the sarcoma-induced lung tumors, having demonstrated a steady overexpression of critical tumor promotion pillars as: (1) a potent transforming and self-autonomy conferring growth factor as TGF-α [50], a prominent oncogene as c-Myc [51], a validated cell proliferation marker as PCNA [52], and two growth factors receptors involved in cancer cells proliferation, immortality, self-autonomy, metastasis, angiogenesis, and reprogramming as EGF-Receptor and VEGF-Receptor 2 [53]. These observations rise the question on what mechanism (s) may be underlying the overexpression of these markers and whether this is associated to an enhanced functional activity. Considering that evidences document that these aberrantly overexpressed proteins in cancer, mechanistically respond to genomic and epigenomic derangements [54-57], anticipate further in-depth analysis of the mice-tumor samples.

The transcriptional expression study contributed to characterize the samples of tumor donor tissues. Despite the mechanical processing of tissue disruption to obtain the CFF, DNA and RNA molecules from tumors homogenates were quantitated, and RNA could be successfully reverse-transcribed. This fact accordingly turns conceivable the hypothesis of some kind of eukaryotic-to-eukaryotic horizontal transfer of genetic or epigenetic ingredient as DNA and/or RNA. Previous studies have shown cells transformation *via* transfection-like uptake of plasma free DNA, derived from colon cancer patients as the subsequent in vivo tumorigenesis when these cells were implanted in mice [58]. Cellular uptake of activated oncogenes DNA transforms cells in vitro and drives tumorigenesis in mice following cells injection [59]. Accordingly, this may represent to the best of our knowledge, the first in vivo tumorigenesis event induced by two different types of tumors crude homogenates.

CFF may also contain some type of tumor-derived extracellular vesicle like exosomes, which are exemplary players in cell-cell communication by conveying genetic and epigenetic messages [60]. The pathogenic engagement of exosomes in human cancer is compelling given their ability to deliver DNA and RNA-tumorigenic signatures (For review see [61]).

Although there are conflicting views regarding the etiopathogenic role of transmissible viruses in the origin of human mammary cancer, for instance [62-64], the hypothesis considering their participation in our experimental scenario was not disregarded. We deem, however, that the timeframe of 4-6 weeks in which both mammary carcinoma and sarcoma homogenates-treated mice debuted with genuine malignancies, seems extremely short for a microorganism to cause cancer [65].

Finally, this study is the third of a series in which the administration of a homogenate from a human pathologic tissue sample from chronic, non-transmissible human diseases, faithfully reproduce in a healthy recipient rodent, traits corresponding to the donor with no cross-species limitation, and in a brief time period. We rely on the existence of a horizontally transferable pathologic tissue memory, founded on abnormal epigenetic controllers that dominantly impose the donor's abnormal phenotype over the host permissive tissue environment. Although one of the limitations of this study is that the mechanisms and actors underpinning these events remain elusive so far, it provides unprecedented evidences and a useful material for translational medical research. We hope that the eventual identification of these transmissible carcinogenesis signatures, may pave roads to unravel novel attributes of cancer pathobiology.

Declaration

References

1. Dou X, et al. Evidence for immortality and autonomy in animal cancer models is often not provided, which causes confusion on key issues of cancer biology. Journal of Cancer. 2020; 11: 2887-2920.

2. Sung H, et al. Global Cancer Statistics 2020: GLOBOCAN Estimates of Incidence and Mortality Worldwide for 36 Cancers in 185 Countries. CA: A Cancer Journal for Clinicians. 2021; 71: 209-249.

3. Komarova NL. Stochastic Modeling of Loss- And Gain-Of-Function Mutations in Cancer. Mathematical Models and Methods in Applied Sciences. 2007; 17: 1647-1673.

4. Alvarado-Ortiz E, et al. Mutant p53 Gain-of-Function: Role in Cancer Development, Progression, and Therapeutic Approaches. Frontiers in Cell and Developmental Biology. 2021; 8.

5. Li Y, et al. Gain-of-Function Mutations: An Emerging Advantage for Cancer Biology. Trends Biochem Sci. 2019; 44: 659-674.

6. Vincent TL and RA Gatenby. An evolutionary model for initiation, promotion, and progression in carcinogenesis. Int J Oncol. 2008; 32: 729-737.

7. Basu AK. DNA damage, mutagenesis and cancer. International journal of molecular sciences. 2018; 19: 970.

8. Dong L, et al. TRIP13 is a predictor for poor prognosis and regulates cell proliferation, migration and invasion in prostate cancer. Int J Biol Macromol. 2019; 121: 200-206.

9. Gupta SC, et al. Regulation of survival, proliferation, invasion, angiogenesis, and metastasis of tumor cells through modulation of inflammatory pathways by nutraceuticals. Cancer metastasis reviews. 2010; 29: 405-434.

10. Zhu S, et al. Integrating conflicting cancer theories by recognizing the roles of epigenetic and genetic alterations in the immediate-cancer-causing genes that establish cellular immortality and autonomy. 2020.

11. Li J and BZ Stanger. How Tumor Cell Dedifferentiation Drives Immune Evasion and Resistance to Immunotherapy. Cancer Res. 2020; 80: 4037-4041.

12. Chao J, S Zhao and H Sun. Dedifferentiation of hepatocellular carcinoma: molecular mechanisms and therapeutic implications. Am J Transl Res. 2020; 12: 2099-2109.

13. Sun X, et al. Exploring the Metabolic Vulnerabilities of Epithelial-Mesenchymal Transition in Breast Cancer. Front Cell Dev Biol. 2020; 8: 655.

14. Das A, MS Nair and SD Peter. Computer-Aided Histopathological Image Analysis Techniques for Automated Nuclear Atypia Scoring of Breast Cancer: a Review. J Digit Imaging. 2020; 33: 1091-1121.

15. Veta M, et al. Breast Cancer Histopathology Image Analysis: A Review. IEEE Transactions on Biomedical Engineering. 2014; 61: 1400-1411.

16. Maley CC, et al. Classifying the evolutionary and ecological features of neoplasms. Nature Reviews Cancer. 2017; 17: 605-619.

17. Duesberg P and A McCormack. Immortality of cancers. Cell Cycle. 2013; 12: 783-802.

18. Cominetti MR, WF Altei and HS Selistre-de-Araujo. Metastasis inhibition in breast cancer by targeting cancer cell extravasation. Breast Cancer (Dove Med Press). 2019; 11: 165-178.

19. Sökeland G and U Schumacher. The functional role of integrins during intra- and extravasation within the metastatic cascade. Molecular Cancer. 2019; 18: 12.

20. Meirson T, H Gil-Henn and AO Samson. Invasion and metastasis: the elusive hallmark of cancer. Oncogene. 2020; 39: 2024-2026.

21. Kreuzaler P, et al. Adapt and conquer: Metabolic flexibility in cancer growth, invasion and evasion. Mol Metab. 2020; 33: 83-101.

22. Szczurek E, et al. A mathematical model of the metastatic bottleneck predicts patient outcome and response to cancer treatment. PLOS Computational Biology. 2020; 16: e1008056.

23. Dillekås H, MS Rogers and O Straume. Are 90% of deaths from cancer caused by metastases? Cancer medicine. 2019; 8: 5574-5576.

24. Taniguchi K and M Karin. NF-κB, inflammation, immunity and cancer: coming of age. Nat Rev Immunol. 2018; 18: 309-324.

25. Tang Z, et al. The cancer exosomes: Clinical implications, applications and challenges. International Journal of Cancer. 2020; 146: 2946-2959.

26. Paul D. The systemic hallmarks of cancer. Journal of Cancer Metastasis and Treatment. 2020; 6: 29.

27. Fouad YA and C Aanei. Revisiting the hallmarks of cancer. American journal of cancer research. 2017; 7: 1016-1036.

28. Hanahan D and RA Weinberg. The hallmarks of cancer. Cell. 2000; 100: 57-70.

29. Suh DH. Book Review: The emperor of all maladies: a biography of cancer. J Gynecol Oncol. 2012; 23: 291-292.

30. Javier RT and JS Butel. The History of Tumor Virology. Cancer Research. 2008; 68: 7693-7706.

31. Berlanga-Acosta J, et al. Intralesional Infiltrations of Cell-Free Filtrates Derived from Human Diabetic Tissues Delay the Healing Process and Recreate Diabetes Histopathological Changes in Healthy Rats. Frontiers in Clinical Diabetes and Healthcare. 2021; 2.

32. Alexandrov LB, et al. Signatures of mutational processes in human cancer. Nature. 2013; 500: 415-421.

33. Sharma S, TK Kelly and PA Jones. Epigenetics in cancer. Carcinogenesis. 2009; 31: 27-36.

34. Lee JE and M-Y Kim. Cancer epigenetics: Past, present and future. Seminars in Cancer Biology. 2021.

35. Issa J-P. Cancer Prevention: Epigenetics Steps Up to the Plate. Cancer Prevention Research. 2008; 1: 219-222.

36. Vandesompele J, et al. Accurate normalization of real-time quantitative RT-PCR data by geometric averaging of multiple internal control genes. Genome Biology. 2002; 3: research0034.1.

37. Ruijter JM, et al. Amplification efficiency: linking baseline and bias in the analysis of quantitative PCR data. Nucleic Acids Res. 2009; 37: e45.

38. Pfaffl MW, GW Horgan and L Dempfle. Relative expression software tool (REST©) for group-wise comparison and statistical analysis of relative expression results in real-time PCR. Nucleic acids research. 2002; 30: e36-e36.

39. Olfert ED, BM Cross and AA McWilliam. Guide to the care and use of experimental animals. 2020; 1. Canadian Council on Animal Care Ottawa.

40. Scudamore CL, N Busk and K Vowell. A simplified necropsy technique for mice: making the most of unscheduled deaths. Laboratory Animals. 2014; 48: 342-344.

41. Nikitin AY, et al. Classification of Proliferative Pulmonary Lesions of the Mouse. Recommendations of the Mouse Models of Human Cancers Consortium. 2004; 64: 2307-2316.

42. Bastami M, et al. Evidences from a systematic review and meta-analysis unveil the role of MiRNA polymorphisms in the predisposition to female neoplasms. International journal of molecular sciences. 2019; 20: 5088.

43. Grünewald TG, et al. Sarcoma treatment in the era of molecular medicine. EMBO Mol Med. 2020; 12: e11131.

44. Damerell V, MS Pepper and S Prince. Molecular mechanisms underpinning sarcomas and implications for current and future therapy. Signal Transduction and Targeted Therapy. 2021; 6: 246.

45. Tang F, et al. Therapeutic applications of histone deacetylase inhibitors in sarcoma. Cancer Treat Rev. 2017; 59: 33-45.

46. Takeuchi A, et al. TTF-1 Expression Predicts the Merit of Additional Antiangiogenic Treatment in Non-squamous Non-small Cell Lung Cancer. Anticancer Res. 2018; 38: 5489-5495.

47. Kuo Y-S, et al. Association of Divergent Carcinoembryonic Antigen Patterns and Lung Cancer Progression. Scientific Reports. 2020; 10: 2066.

48. Nguyen C, et al. Pulmonary Atypical Adenomatous Hyperplasia: Diagnostic and Therapeutic Implications. Cureus. 2019; 11: e6079.

49. Katt ME, AD Wong and PC Searson. Dissemination from a Solid Tumor: Examining the Multiple Parallel Pathways. Trends Cancer. 2018; 4: 20-37.

50. Kavanagh S, et al. TGF-α expression in myeloid malignancies. J Clin Pathol. 2016; 69: 543-546.

51. Madden SK, et al. Taking the Myc out of cancer: toward therapeutic strategies to directly inhibit c-Myc. Molecular Cancer. 2021; 20: 3.

52. Cardano M, C Triboli and E Prosperi. Targeting Proliferating Cell Nuclear Antigen (PCNA) as an Effective Strategy to Inhibit Tumor Cell Proliferation. Curr Cancer Drug Targets. 2020; 20: 240-252.

53. Mourad AAE, et al. EGFR/VEGFR-2 dual inhibitor and apoptotic inducer: Design, synthesis, anticancer activity and docking study of new 2-thioxoimidazolidin-4one derivatives. Life Sci. 2021; 277: 119531.

54. Chakravarthi BV, S Nepal and S Varambally. Genomic and Epigenomic Alterations in Cancer. Am J Pathol. 2016; 186: 1724-1735.

55. Baylin SB and PA Jones. Epigenetic Determinants of Cancer. Cold Spring Harb Perspect Biol. 2016; 8.

56. Gonzalez-Conchas GA, et al. Epidermal growth factor receptor overexpression and outcomes in early breast cancer: A systematic review and a meta-analysis. Cancer Treatment Reviews. 2018; 62: 1-8.

57. Wee P and Z Wang. Epidermal growth factor receptor cell proliferation signaling pathways. Cancers. 2017; 9: 52.

58. García-Olmo DC, et al. Cell-free nucleic acids circulating in the plasma of colorectal cancer patients induce the oncogenic transformation of susceptible cultured cells. Cancer Res. 2010; 70: 560-567.

59. Bergsmedh A, et al. Horizontal transfer of oncogenes by uptake of apoptotic bodies. Proceedings of the National Academy of Sciences. 2001; 98: 6407-6411.

60. Maia J, et al. Exosome-Based Cell-Cell Communication in the Tumor Microenvironment. Front Cell Dev Biol. 2018; 6: 18.

61. Mashouri L, et al. Exosomes: composition, biogenesis, and mechanisms in cancer metastasis and drug resistance. Molecular Cancer. 2019; 18: 75.

62. Lawson JS and WK Glenn. Catching viral breast cancer. Infectious agents and cancer. 2021; 16: 1-11.

63. Lawson JS and WK Glenn. Multiple oncogenic viruses are present in human breast tissues before development of virus associated breast cancer. Infectious agents and cancer. 2017; 12: 1-8.

64. Gannon O, et al. Viral infections and breast cancer-A current perspective. Cancer letters. 2018; 420: 182-189.

65. Lawson JS, WK Glenn and NJ Whitaker. Human papilloma viruses and breast cancer–assessment of causality. Frontiers in Oncology. 2016; 6: 207.